materials

MDPI

Article

Direct Growth of CuO Nanorods on Graphitic Carbon Nitride with Synergistic Effect on Thermal Decomposition of Ammonium Perchlorate

Linghua Tan [1,2,*,†], Jianhua Xu [2,†], Shiying Li [2], Dongnan Li [1], Yuming Dai [3], Bo Kou [3] and Yu Chen [3]

1 National Special Superfine Power Engineering Research Center, Nanjing University of Science and Technology, Nanjing 210094, China; joshldn@163.com
2 School of Chemical Engineering, Nanjing University of Science and Technology, Nanjing 210094, China; xujianhua931118@163.com (J.X.); lishiying0613@163.com (S.L.)
3 Jiangsu Key Laboratory of Advanced Structural Materials and Application Technology, School of Materials Engineering, Nanjing Institute of Technology, Nanjing 211167, China; dym@njit.edu.cn (Y.D.); koutianbo@hotmail.com (B.K.); cy_5432@163.com (Y.C.)
* Correspondence: tanlh@njust.edu.cn; Tel.: +86-25-8431-5042
† These authors contributed equally to this work.

Academic Editor: Homayoun Hadavinia
Received: 26 March 2017; Accepted: 26 April 2017; Published: 2 May 2017

Abstract: Novel graphitic carbon nitride/CuO (g-C_3N_4/CuO) nanocomposite was synthesized through a facile precipitation method. Due to the strong ion-dipole interaction between copper ions and nitrogen atoms of g-C_3N_4, CuO nanorods (length 200–300 nm, diameter 5–10 nm) were directly grown on g-C_3N_4, forming a g-C_3N_4/CuO nanocomposite, which was confirmed via X-ray diffraction (XRD), transmission electron microscopy (TEM), field emission scanning electron microscopy (FESEM), and X-ray photoelectron spectroscopy (XPS). Finally, thermal decomposition of ammonium perchlorate (AP) in the absence and presence of the prepared g-C_3N_4/CuO nanocomposite was examined by differential thermal analysis (DTA), and thermal gravimetric analysis (TGA). The g-C_3N_4/CuO nanocomposite showed promising catalytic effects for the thermal decomposition of AP. Upon addition of 2 wt % nanocomposite with the best catalytic performance (g-C_3N_4/20 wt % CuO), the decomposition temperature of AP was decreased by up to 105.5 °C and only one decomposition step was found instead of the two steps commonly reported in other examples, demonstrating the synergistic catalytic activity of the as-synthesized nanocomposite. This study demonstrated a successful example regarding the direct growth of metal oxide on g-C_3N_4 by ion-dipole interaction between metallic ions, and the lone pair electrons on nitrogen atoms, which could provide a novel strategy for the preparation of g-C_3N_4-based nanocomposite.

Keywords: g-C_3N_4; CuO; Nanocomposite; catalysis; synergistic effect

1. Introduction

Recently, graphitic carbon nitride (g-C_3N_4) has drawn considerable attention due to its unusual physical and chemical properties, which show great potential for the application in many aspects. g-C_3N_4 is metal-free, and has multiple structural defects, good thermal and chemical stability, and tunable electronic structure. More importantly, g-C_3N_4 is cost-effective and environmentally friendly. All these make g-C_3N_4 become a novel and promising form of catalysis and catalytic support [1–8]. To broaden the application of the g-C_3N_4-based nanocomposite, compounding functional nano-sized metal oxide materials with g-C_3N_4 has been of interest over recent years. The synergy of two functional materials will result in improved properties of the nanocomposite that will have a wider range of applications [9–12].

Specifically, Sridharan and his co-workers [13] reported the coupling of g-C_3N_4 with TiO_2 by utilizing a thermal transformation methodology. With higher photocatalytic ability, the prepared composite greatly improved the degradation of methylene blue. Additionally, g-C_3N_4/CeO_2 was prepared for the evaluation of its potential application in the hydrogen production by photocatalysis, and degradation of methylene blue [14,15]. g-C_3N_4/Bi_2WO_6 was also studied to explore its excellent properties [16–20]. For example, Li's group [16] synthesized a series of g-C_3N_4/Bi_2WO_6 composites through a facile in situ hydrothermal approach, which demonstrated greatly enhanced responses to visible light. The selective reduction of CO_2 to CO was remarkably enhanced. Analogously, Sierra et al. [20] developed a Bi/Bi_2WO_6/g-C_3N_4 ternary composite via thermal reduction of Bi_2WO_6 with g-C_3N_4. Owing to its remarkable red-shift up to 620 nm, Bi/Bi_2WO_6/g-C_3N_4 could catalyze the degradation of methylene blue contaminants under visible light.

CuO is a typical p-type semiconductor that has been widely applied in photoelectric materials, gas sensors and catalysis [21,22]. The preparation of CuO nanostructures has received much attention in recent years [23,24]. Zhu et al. [25] prepared a CuO:GO nanocomposite by a facile chemical method without the utilization of any templates or surfactants. Due to the good dispersion of CuO nanocrystals on GO nanosheets, the obtained CuO:GO nanocomposite showed a synergistic effect for the thermal decomposition of AP. Zabilskiy's group [26] prepared a series of CuO crystals supported on CeO_2 nanospheres using a glycothermal approach. The synthesized CuO/CeO_2 exhibited very promising activity and stability, which could be effectively applied to the catalysis of N_2O decomposition. Recently, Wang's group reported on a new synthetic approach for the preparation of porous nanorod-type graphitic carbon nitride/CuO composites using a Cu-melamin supramolecular framework as a precursor [27]. These works have focused more on the control of the morphology of g-C_3N_4 than on that of CuO. Specifically, due to the three-dimensional hydrogen-bond (N—H···N) directions which guide the condensation of melamine molecules in the Cu-melamin precursor, the as-prepared CuO-g-C_3N_4 showed a porous nanorod morphology consisting of CuO nanoparticles spread on the surface of rod-shaped g-C_3N_4. However, the high reaction temperature (up to 550 °C) would lead to the serious sintering of CuO nanoparticles, which could affect the catalytic activity of the CuO-g-g-C_3N_4. Based on the above analysis, in order to obtain a novel g-C_3N_4/CuO nanocomposite with synergistic effect, the CuO nanoparticles were made to be uniformly dispersed on g-C_3N_4. Herein, we report on an improved strategy for the preparation of CuO nanorods well-dispersed g-C_3N_4 nanocomposite via the direct growth of CuO nanorods on g-C_3N_4, using a facile precipitation method (Scheme 1).

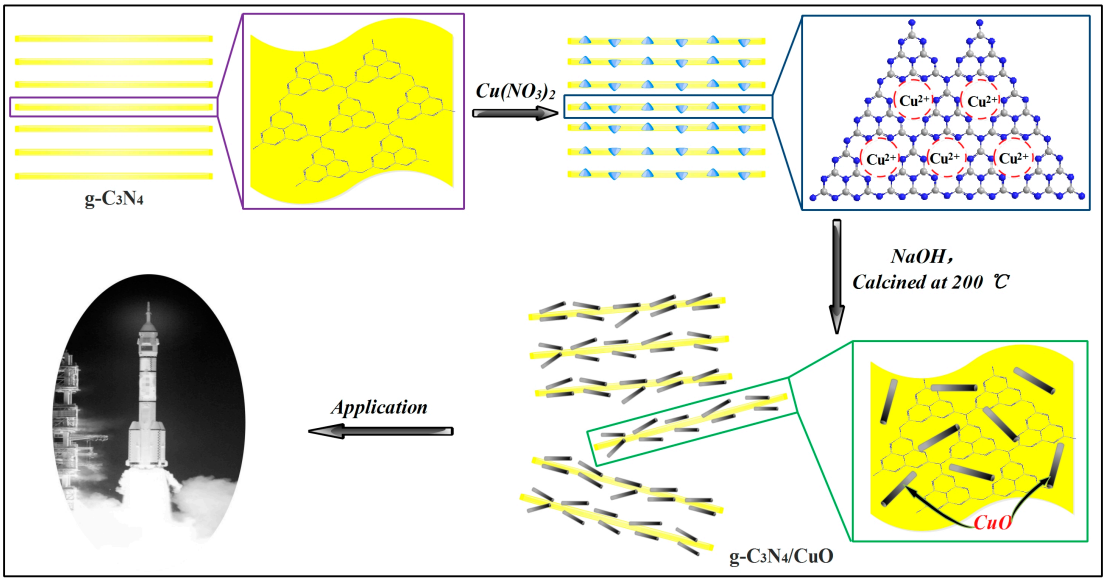

Scheme 1. Illustration of the formation and application of the g-C_3N_4/CuO nanocomposite.

Ammonium perchlorate (AP), which accounts for 60% of the total mass of the propellant, is the most common oxidant in composite solid propellants [28]. The properties of solid propellants mostly depend on reaction rate, high-temperature decomposition, and the activation energy of AP thermal decomposition. Thus, exothermic heat and lower high-temperature decomposition (HTD) play an important role in the utilization of AP [29]. Up to now, as a transition metal oxide, CuO was demonstrated to be a promising catalyst for the thermal decomposition of AP [25]. Moreover, our group confirmed that g-C_3N_4 can also accelerate the thermal decomposition process [30]. It was anticipated that the direct growth of CuO on g-C_3N_4 will not only avoid the agglomeration of nano-sized CuO, but also efficiently accelerate the electron transfer rate between them. Thus, the thermal decomposition process of AP could be markedly accelerated in the presence of the novel g-C_3N_4/CuO catalyst.

2. Experimental

2.1. Materials

All the reagents were of analytical grade and used as received without further purification. Melamine, sodium hydroxide, cupric nitrate trihydrate and ethanol were all purchased from Sinopharm (Beijing, China). Distilled water was used throughout the experiment.

2.2. Preparation of g-g-C_3N_4/CuO Nanocomposite

Firstly, g-C_3N_4 solid was synthesized by heating melamine in a muffle furnace (Hefei Ke Jing Materials Technology Co., Ltd., Hefei, China) at 520 °C for two hours at a heating rate of 50 °C min^{-1} with air, the solid was then ground with agate mortar to obtain g-C_3N_4 powder. The product was washed with distilled water three times and dried at 70 °C [30].

Secondly, the g-C_3N_4/CuO nanocomposite was synthesized using a facile precipitation method [31]. The g-C_3N_4/CuO nanocomposite with differing CuO contents (5, 10, 20, 30, 50 wt %) were prepared and labeled as g-C_3N_4/x wt % CuO (x = 5, 10, 20, 30, 50). A typical experiment for the synthesis of g-C_3N_4/20 wt % CuO catalyst is as follows: 0.32 g of g-C_3N_4 was dispersed in 60 mL deionized water by ultrasonication for 30 min. Afterwards, 0.242 g $Cu(NO_3)_2{\cdot}3H_2O$ (analytically pure) was added into the solution, and then the obtained dispersion was stirred for another 20 min. Subsequently, 10 mL sodium hydroxide solution (1 mol·L^{-1}) was added dropwise with stirring. The mixture was then stirred at room temperature for two hours, then collected, washed with deionized water and alcohol, and dried. Finally, the mixture was calcined in a muffle furnace at 200 °C for two hours, to obtain the g-C_3N_4/CuO nanocomposite. CuO without g-C_3N_4 was also obtained using the same method under the same conditions.

2.3. Characterization

Unless otherwise indicated, g-C_3N_4/CuO nanocomposite containing 20 wt % CuO was used as a representative for characterization.

The crystalline phases of products were analyzed by X-ray diffraction (XRD) using a Rigaku Ultima-IV advanced X-ray diffractometer (Rigaku, Tokyo, Japan) with Cu Kα irradiation (λ = 0.15406 nm) within the range of 2θ = 10°–90°. The morphology and structure of the as-synthetized nanocomposite was observed by field emission scanning electron microscopy (FESEM, Zeiss MERLIN Compact, Jena, Germany) and transmission electron microscopy (TEM, Philips Tecnai 12, Amsterdam, The Netherlands). X-ray photoelectron spectra (XPS) were recorded on a PHI Quantera II X-ray photoelectron spectrometer (Chigasaki, Japan), using Al Kα radiation as the excitation source.

2.4. Catalytic Activity Measurement

For study of the catalytic performance of g-C_3N_4/CuO nanocomposite on the thermal decomposition of AP, AP powder mixed with g-C_3N_4, CuO, and g-C_3N_4/CuO were prepared.

For sample preparation for catalytic research, 0.01 g g-C_3N_4, CuO or g-C_3N_4/CuO was mixed with 0.49 g AP in ethanol, stirred for one hour, and then dried at 60 °C for one hour.

The resulting powder was determined by differential thermal analysis (DTA) (NETZSCH Instrument 404 PC, Selb, Germany) and thermal gravimetric analysis (TGA) (Beijing Hengjiu Instrument HTG-1, Beijing, China) at a heating rate of 10 °C min^{-1} (from 100–500 °C) under an N_2 atmosphere.

3. Result and Discussion

3.1. Morphology and Textural Property

The crystal structures of pure g-C_3N_4, CuO, and g-C_3N_4/CuO nanocomposite with various CuO contents were studied by XRD. As illustrated in Figure 1a, the g-C_3N_4 sample had a characteristic peak at 27.4° and 13.2°, which could be indexed by the hexagonal g-C_3N_4 (JCPDS87-1526) as the (002) and (100) diffraction plane peaks, corresponding to the interlayer stacking of aromatic segments with a distance of 0.326 nm, and the in-plane structural packing motif, respectively [32,33]. The diffraction peaks of the obtained CuO were indexed to the monoclinic phase of CuO (JCPDS05-0661) [34]. The diffraction peaks at 32.4°, 35.6°, 38.8°, 48.7°, 53.5°, 58.3°, 61.5°, 66.1°, 68.1°, 72.4°, 75.2° were observed (Figure 1a), corresponding to (1, 1, 0), (−1, 1, 1), (1, 1, 1), (−2, 0, 2), (0, 2, 0), (2, 0, 2), (−1, 1, 3), (3, 1, −1), (2, 2, 0), (3, 1, 1) and (2, 2, −2) [35]. The g-g-C_3N_4/CuO nanocomposite exhibited diffraction peaks corresponding to both g-C_3N_4 and CuO, reflecting the presence of two phases, and no other impurity peaks were observed. The enlarged profiles of the g-C_3N_4, CuO and all the g-C_3N_4/CuO nanocomposites are shown in Figure 1b. With an increased content of CuO in the g-C_3N_4/CuO nanocomposite, the characteristic peaks of g-C_3N_4 were gradually decreased, and the diffraction peaks of CuO were all slowly increased, indicating the successful synthesis of g-C_3N_4/CuO nanocomposite [36]. Nevertheless, the (002) reflection peak of the laminated g-C_3N_4 gradually shifted to a small angle direction along with an increased loading percentage of CuO nanorods on g-C_3N_4, which indicated that a certain number of CuO nanorods were grown in situ on the inter-lamination of g-C_3N_4, resulting in the increase of inter-layer spacing [37].

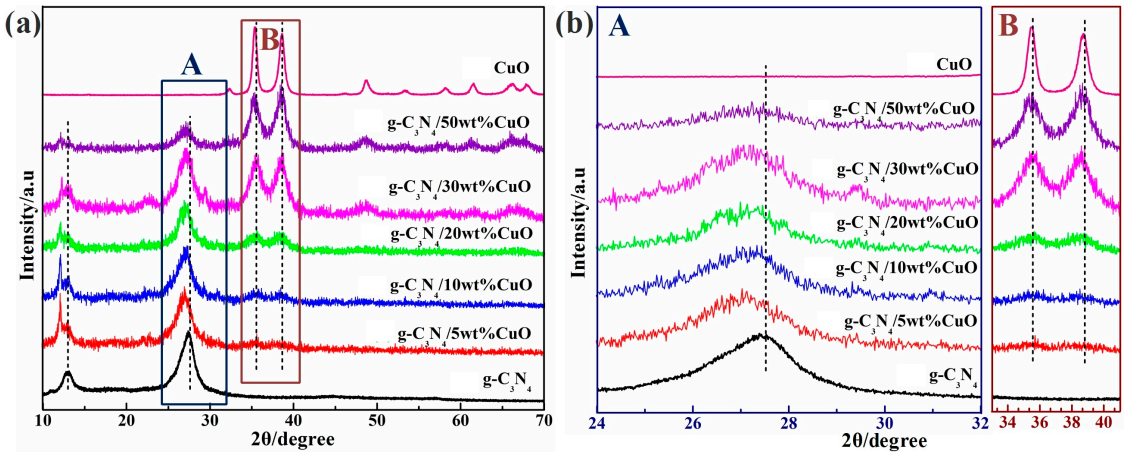

Figure 1. (**a**) X-ray diffraction (XRD) patterns of pure g-C_3N_4, CuO and g-C_3N_4/CuO nanocomposites with various contents of CuO; (**b**) Enlarged profiles of the selected area in Figure 1a.

The morphology of g-C_3N_4, CuO and g-C_3N_4/CuO nanocomposite (20 wt % CuO as a representative) was investigated by TEM and FESEM, and the TEM result is described in Figure 2. Figure 2a confirmed that g-C_3N_4 displayed a 2D laminated structure, which is similar to its graphite analogue, containing several stacking layers [38]. As shown in Figure 2b,c, pure CuO showed a dense agglomeration of rough nanoscale rods and spherical particles with an average diameter of

5–10 nm. However, the morphology of g-C_3N_4/CuO was obviously different from pure g-C_3N_4 and CuO. Figure 2d clearly demonstrated that CuO nanorods (labeled with red arrows) were well dispersed in g-C_3N_4. The light portion was g-C_3N_4, and the nanorod-shaped dark portion was CuO, which confirmed that CuO nanorods were directly grown on g-C_3N_4. Previous studies have indicated that g-C_3N_4 exhibits a strong ability to capture cations via an ion-dipole interaction between cations and lone pairs of electrons on nitrogen atoms of g-C_3N_4 [39,40]. Thus, after dispersing the g-C_3N_4 into the solution with cupric ions, the cupric ions could be captured and randomly dispersed into the framework of g-C_3N_4 (Scheme 1). In this case, upon the addition of hydroxide solution, the nano-$Cu(OH)_2$ could be formed in situ because of the ion-dipole interaction, efficiently avoiding agglomeration. In addition, compared with the bulk g-C_3N_4 from Figure 2a, the color of g-C_3N_4 in g-C_3N_4/CuO nanocomposite (Figure 2d,e) was brighter, which indicated thinner lamellar thickness. These results demonstrated that the interlayer-formed CuO nanorods (synthesized by the calcination of as-prepared $Cu(OH)_2$ at 200 °C) in return caused the partial exfoliation of the bulk g-C_3N_4, which was also supported by XRD results (Figure 1). Figure 2e,f show the TEM images with high magnification of the g-C_3N_4/CuO nanocomposite. We observed that the diameter of CuO nanorods ranged between 5–10 nm and the length was approximately 200–300 nm. As shown in Figure 2e, the overlapping phenomenon of CuO nanorods resulted from their simultaneous existence on the surface and inter-lamination of g-C_3N_4.

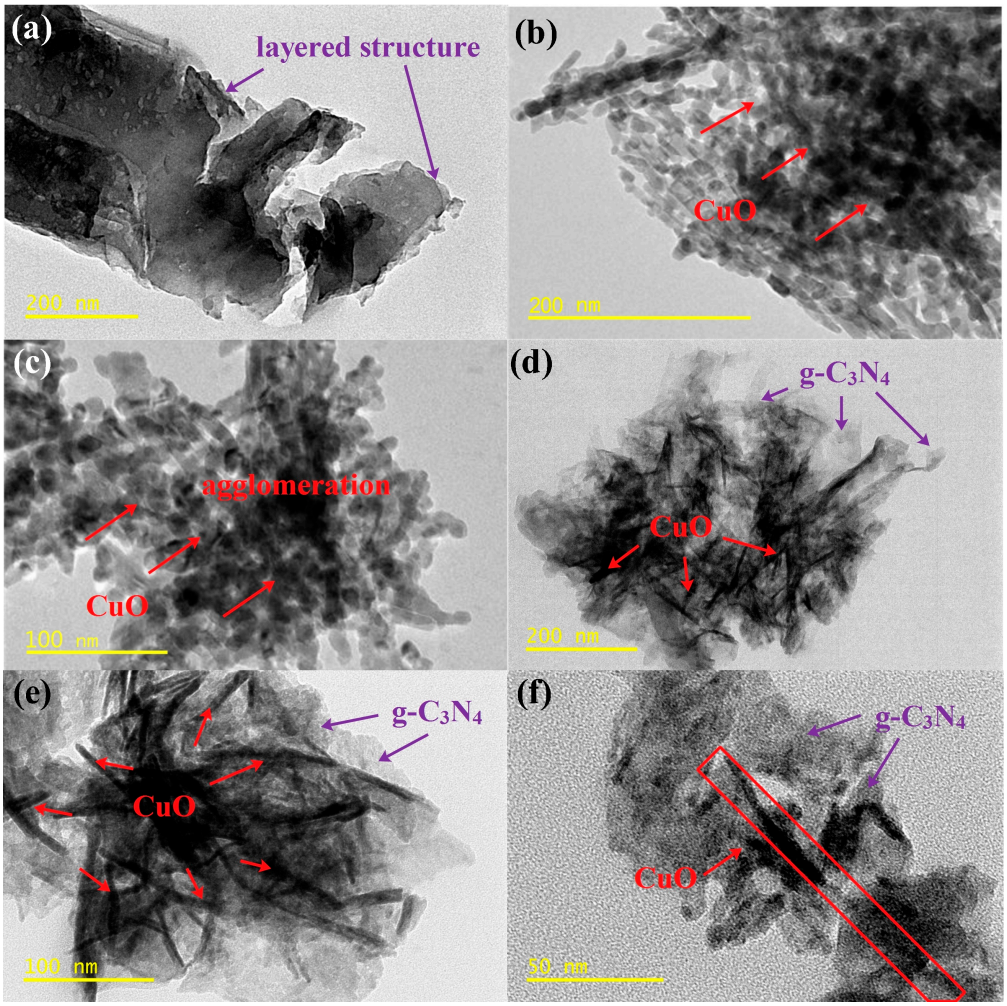

Figure 2. Transmission electron microscopy (TEM) images of (**a**) pure g-C_3N_4, (**b**,**c**) CuO, and (**d**–**f**) g-C_3N_4/20 wt % CuO nanocomposite.

Figure 3a further revealed that the pure g-C_3N_4 had loose laminated structures adhered between interlaminations [41]. From Figure 3b,c, CuO nanorods with a diameter of about 5–10 nm, and a length of 200–300 nm (labelled with red frame) were found to be dispersed on g-C_3N_4. We also employed energy dispersive spectrometer (EDS) to conduct elemental analysis on the nanocomposite, and characteristic peaks corresponding to C, N, Cu, and O were present in the EDS spectrum (Figure 3d). In order to further investigate the elemental distribution of the g-C_3N_4/CuO nanocomposite, the elemental mappings of C, N, Cu and O were also performed by EDS area scanning (Figure 3e). The maps of C, N, Cu and O were well defined, with sharp contrast. The maps of C and N showed C and N signals, respectively, indicating the definite existence of g-C_3N_4. The profile of Cu was similar to that of O, demonstrating the homogeneous distribution of CuO nanorods on g-C_3N_4. All these demonstrated the successful decorating of g-C_3N_4 with CuO nanorods.

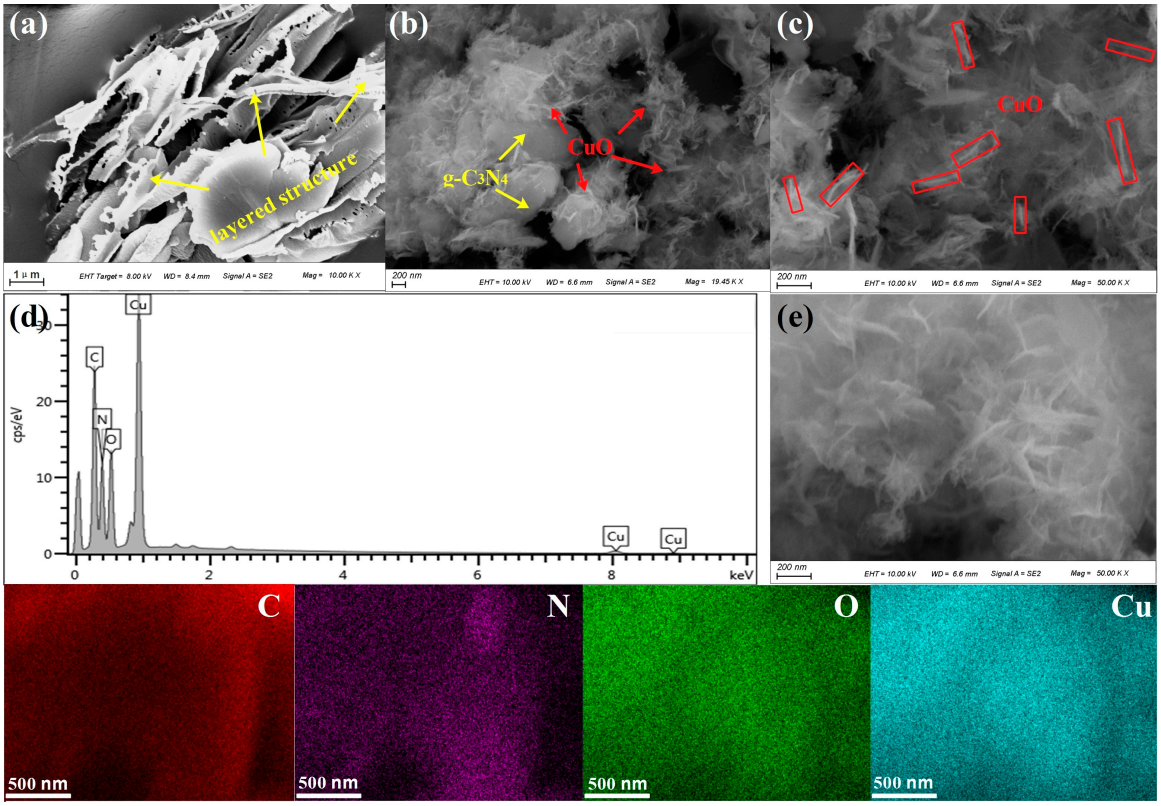

Figure 3. Field emission scanning electron microscopy (FESEM) images of (**a**) pure g-C_3N_4, (**b**,**c**) g-C_3N_4/CuO nanocomposite; (**d**) energy dispersive spectrometer (EDS) spectrum and (**e**) elemental mappings of the g-C_3N_4/20 wt % CuO nanocomposite.

XPS was performed to further confirm the composition and the chemical states of the nanocomposite. The results obtained in the XPS analysis were corrected by referencing the C1s line to 284.6 eV. The full scan of the XPS spectra of g-C_3N_4 (Figure 4a) showed that characteristic peaks corresponding to C, N, O and Si elements were found. The existence of the O1s peak was due to the existence of O_2 on the surface of the sample [42], and the existence of Si2p was attributed to the introduction of trace SiO_2 during grinding. Meanwhile, characteristic peaks corresponding to C, N, O, and Cu were found in the full scan spectra of g-C_3N_4/CuO, and no other peaks could be assigned. All these demonstrated the successful preparation of the g-C_3N_4/CuO nanocomposite. Figure 4b,c are high-resolution XPS spectra of the C1s, and N1s. There were two peaks present in the C1s spectrum of g-C_3N_4, and the peak at 284.6 eV could be ascribed to the surface adventitious reference carbon, whereas the binding energy at 288.3 eV was corresponding to sp^2-hybrid carbon of

the N–C=N group [43]. The C1s spectrum of g-C_3N_4/CuO was similar to that of g-C_3N_4, while the blue shift (0.2 eV) of the binding energy at 288.1 eV indicated the interaction between g-C_3N_4 and CuO. As for the N1s high-resolution spectrum of g-C_3N_4, three binding energy peaks at 398.5, 399.2 and 400.6 eV could be assigned to the aromatic N(C=N–C), tertiary N(N–$(C)_3$), and the N atom on C–N–H group, respectively [44,45]. The blue shift (0.1 eV) of the aromatic N(C=N–C) in the N1s spectrum of g-C_3N_4/CuO (Figure 4c) also supported the strong interaction between g-C_3N_4 and CuO.

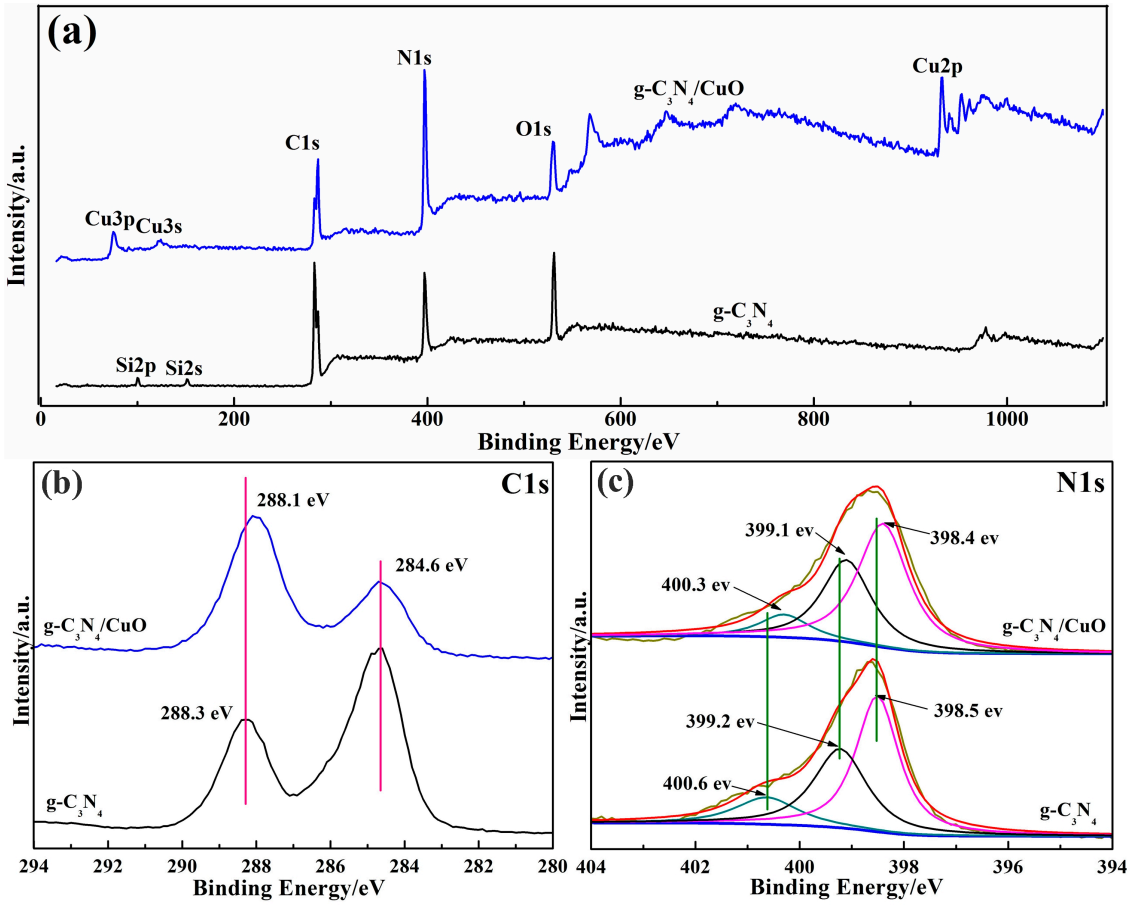

Figure 4. X-ray photoelectron spectra (XPS) of g-C_3N_4 and g-C_3N_4/20 wt % CuO nanocomposite: (**a**) full scan; (**b**) high resolution C1s; (**c**) high resolution N1s.

3.2. Catalytic Activity of Nanocomposite Materials for Ammonium Perchlorate (AP) Decomposition

The thermal decomposition of AP was employed to evaluate the catalytic effect of g-C_3N_4/CuO nanocomposite. Specifically, AP in the absence and presence of 2 wt % pure g-C_3N_4, CuO, and g-C_3N_4/CuO (various content of CuO from 5 to 50 wt % versus g-C_3N_4/CuO), respectively, were utilized to investigate its thermal decomposition by differential thermal analysis (DTA) and thermal gravimetric analysis (TGA), and the results were illustrated in Figures 5 and 6. The thermal decomposition process of AP in the absence of catalyst exhibited two exothermic peaks at 326.3 and 425.1 °C, corresponding to the low and high temperature decomposition stages [46], and one endothermic peak at 248.3 °C, which was the crystal transformation temperature of AP [47] (Figure 5). The addition of catalyst led to significant change in both high and low decomposition temperatures, while did not affect the crystal transformation temperature. When treated with 2 wt % CuO and 2 wt % g-C_3N_4 separately, the high decomposition temperature (HTD) of AP was decreased by 84.6 °C, and 27.0 °C, suggesting that pure CuO exhibited higher catalytic performance on thermal decomposition of AP than pure g-C_3N_4, which is in accordance with the literature [48]. Besides, with

CuO content increased from 5 to 20 wt % in the g-C_3N_4/CuO nanocomposite, the HTD of AP decreased gradually. Specifically, upon the addition of 2 wt % g-C_3N_4/20 wt % CuO nanocomposite as a catalyst, the HTD of AP showed a maximum decrease of 105.5 °C, and only one peak corresponding to decomposition temperature was present in the spectrum, which was presumably due to the merging of high and low decomposition temperatures. In the case of the g-C_3N_4/CuO nanocomposite, CuO were all nano-sized and well dispersed throughout the micron-sized g-C_3N_4. Previous studies have indicated that active sites exposed on the surface of nanocomposite would significantly increase the enhancement well dispersed nano-component concentrations to some extent [49,50]. Thus, g-C_3N_4/20 wt % CuO exhibited higher catalytic performance on the thermal decomposition of AP than g-C_3N_4/10 wt % CuO and g-C_3N_4/5 wt % CuO, respectively. Meanwhile, on account of the partial agglomeration of CuO nanorods on g-C_3N_4 with the percentage of CuO being more than 20 wt % versus g-C_3N_4/CuO (g-C_3N_4/30 wt % CuO and g-C_3N_4/50 wt % CuO), the catalytic efficacy of the g-C_3N_4/CuO nanocomposite was decreased (Table 1); this was accompanied by the recurrence of two exothermic peaks corresponding to high and low decomposition temperatures, respectively.

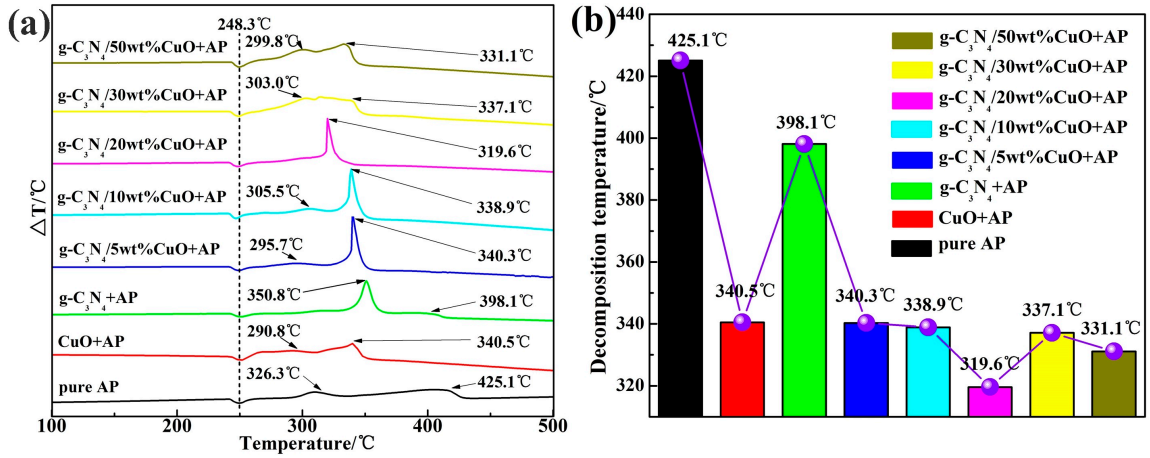

Figure 5. (**a**) Differential thermal analysis (DTA) curves of ammonium perchlorate (AP) in the absence and presence of a catalyst; (**b**) histogram of the corresponding high decomposition temperature.

The TG and DTG curves in Figure 6 showed that the decomposition process of AP has two platforms, indicating that there are two weight loss steps of AP from 100 to 500 °C [51]. It was also discovered that the initial and final weight-loss decomposition temperatures decreased in the presence of all independent catalysts (Figure 6a). In particular, with 2 wt % g-C_3N_4 and 2 wt % CuO, separately, both the two weight-loss decomposition temperatures of AP were decreased, and the decomposition process still exhibited two platforms corresponding to initial and final weight-loss decomposition. However, it should be noted that the addition of g-C_3N_4/CuO reduced the temperature span between the initial and final weight-loss decomposition temperatures, and the span disappeared with 20 wt % CuO (versus g-C_3N_4/CuO) added, resulting in a merge into one peak at 318.6 °C (maximum decrease by 128.5 °C) in the spectrum (Figure 6b), which is consistent with the observation from DTA. Meanwhile, the recurrence of two peaks corresponding to the initial and final weight-loss decomposition temperatures, when treated with g-C_3N_4/CuO containing more than 20 wt % CuO, implies that the catalytic efficacy of the g-C_3N_4/CuO nanocomposite decreased (Table 1). Overall, our observations indicated that g-C_3N_4 and CuO show synergistic catalytic effects on the thermal decomposition of AP.

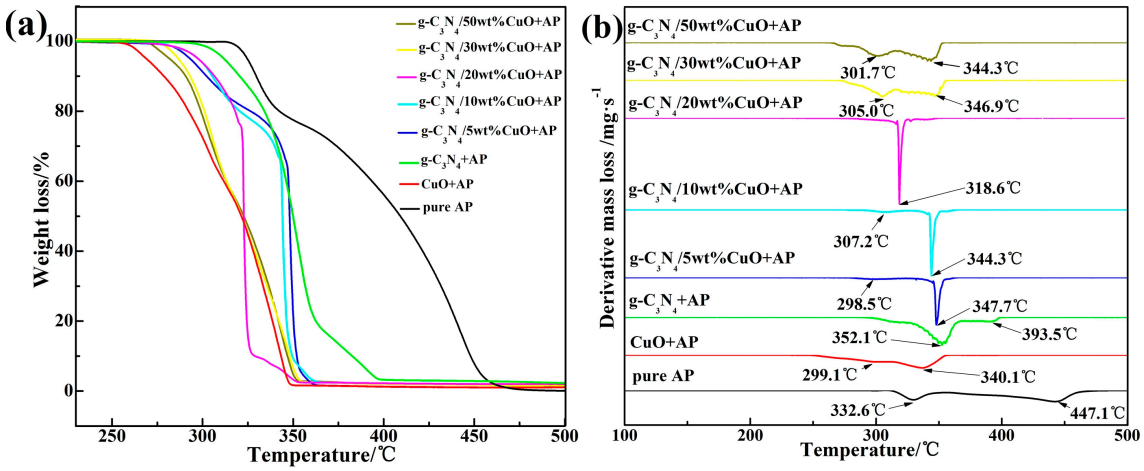

Figure 6. Thermal gravimetric analysis (TGA) (**a**) and derivative thermogravimetric analysis (DTG) (**b**) curves of ammonium perchlorate (AP) in the absence and presence of catalysts.

Table 1. High decomposition temperature and high weight-loss decomposition temperature of ammonium perchlorate (AP) in the absence and presence of different catalyst.

Sample	High Decomposition Temperature (°C)	High Weight-Loss Decomposition Temperature (°C)
Pure AP	425.1	447.1
CuO + AP	340.5	340.1
g-C_3N_4 + AP	398.1	393.5
g-C_3N_4/5 wt % CuO + AP	340.3	347.7
g-C_3N_4/10 wt % CuO + AP	338.9	344.3
g-C_3N_4/20 wt % CuO + AP	319.6	318.6
g-C_3N_4/30 wt % CuO + AP	337.1	346.3
g-C_3N_4/50 wt % CuO + AP	331.1	344.3

The proposed thermal decomposition process of AP catalyzed by g-C_3N_4/CuO was also studied. The low temperature decomposition was a solid-gas heterogeneous reaction, which included a proton transfer to form NH_3 and $HClO_4$, the adsorption of NH_3 and $HClO_4$ in the porous structure, the decomposition of $HClO_4$, and a subsequent reaction with NH_3 [30]. The high temperature gas-phase decomposition reaction included the oxidation of NH_3 by $HClO_4$ in the gas phase [52].

Previous studies demonstrated that proton transfer was the most important process of the thermal decomposition of AP. Indeed, the as-prepared g-C_3N_4/CuO nanocomposite effectively promoted proton transfer.

On one hand, Chen et al. illustrated that the surface O^{2-} species of the CuO nanorod were likely to be proton traps which could react with NH_4^+ easily and then promote the process of proton transfer [53]. On the other hand, due to the unique surface structure of g-C_3N_4 that could be considered to be a Lewis base [54], $HClO_4$ (generated from proton transfer reaction) could be absorbed on the surface of g-C_3N_4 via a Lewis acid-base interaction, leading to the separation of $HClO_4$ from the pores of AP, and then resulting in a decrease of activation energy, thus accelerating the thermal decomposition of AP [55,56]. In summary, by combining the functions of g-C_3N_4 and CuO, the as-prepared g-C_3N_4/CuO nanocomposite would promote proton transfer effectively, and accelerating the thermal decomposition process of AP.

4. Conclusions

The novel nanocomposite g-C_3N_4/CuO, was synthesized through a facile precipitation method, and fully characterized using various methods. Specifically, on account of the ion-dipole interaction

between cupric ions and long pair electrons on the nitrogen atoms of g-C_3N_4, CuO nanorods with diameter in the range of 5–10 nm and length of 200–300 nm were directly grown on g-C_3N_4. Moreover, g-C_3N_4/CuO greatly accelerated the thermal decomposition of AP. Upon addition of g-C_3N_4/CuO, the decomposition temperature of AP was decreased by up to 105.5 °C, and only one decomposition step was found, demonstrating synergetic catalytic activity of g-C_3N_4 and CuO. g-C_3N_4 was decorated with other promising metal oxides, which could broaden the application of g-C_3N_4. This potential application is currently being examined by our group.

Acknowledgments: This work was supported by the Science Foundation of Nanjing Institute of Technology (ZKJ201402) and (ZKJ201501), the Natural Science Foundation of Jiangsu Province (BK20160773), the National Natural Science Foundation of China (NSFC 21603102) and the Priority Academic Program Development of Jiangsu Higher Education Institutions (PAPD).

Author Contributions: All the authors have been collaborating with each other to obtain a high-quality research work. Linghua Tan and Jianhua Xu conceived and designed the experiments; Shiying Li and Dongnan Li performed the preparation experiments; Yuming Dai and Bo Kou analyzed the XRD and XPS data; Jianhua Xu and Yu Chen contributed the microstructure characterization of samples in TEM, FESEM as well as EDS; Jianhua Xu and Dongnan Li performed the catalytic experiments about the AP's decomposition. Linghua Tan wrote the paper and Shiying Li contributed the revision of the paper.

Conflicts of Interest: The authors declare no conflict of interest.

References

1. Wang, X.C.; Maeda, K.; Thomas, A.; Takanabe, K.; Xin, G.; Carlsson, J.M.; Domen, K.; Antonietti, M. A metal-free polymeric photocatalyst for hydrogen production from water under visible light. *Nat. Mater.* **2008**, *8*, 76–80. [CrossRef] [PubMed]
2. Lau, V.W.H.; Mesch, M.B.; Duppel, V.; Blum, V.; Senker, J.; Lotsch, B.V. Low-molecular-weight carbon nitrides for solar hydrogen evolution. *J. Am. Chem. Soc.* **2015**, *137*, 1064–1072. [CrossRef] [PubMed]
3. Liu, J.; Wang, H.Q.; Antonietti, M. Graphitic carbon nitride "reloaded": Emerging applications beyond (photo) catalysis. *Chem. Soc. Rev.* **2016**, *45*, 2308–2326. [CrossRef] [PubMed]
4. Ong, W.J.; Tan, L.L.; Yun, H.N.; Yong, S.T.; Chai, S.P. Graphitic carbon nitride (g-C_3N_4)-based photocatalysts for artificial photosynthesis and environmental remediation: Are we a step closer to achieving sustainability? *Chem. Rev.* **2016**, *116*, 7159–7329. [CrossRef] [PubMed]
5. Yin, S.M.; Han, J.Y.; Zhou, T.H.; Xu, R. Recent progress in g-C_3N_4 based low cost photocatalytic system: Activity enhancement and emerging applications. *Catal. Sci. Technol.* **2015**, *5*, 5048–5061. [CrossRef]
6. Zhao, Z.W.; Sun, Y.J.; Dong, F. Graphitic carbon nitride based nanocomposites: A review. *Nanoscale* **2014**, *7*, 15–37. [CrossRef] [PubMed]
7. Dante, R.C.; Martín-Ramos, P.; Navas-Gracia, L.M.; Sánchez-Arévalo, F.M.; Martín-Gil, J. Polymeric carbon nitride nanosheets. *J. Macromol. Sci. B* **2013**, *52*, 623–631. [CrossRef]
8. Dante, R.C.; Martín-Ramos, P.; Correa-Guimaraes, A.; Martín-Gil, J. Synthesis of graphitic carbon nitride by reaction of melamine and uric acid. *Mater. Chem. Phys.* **2011**, *130*, 1094–1102. [CrossRef]
9. Kong, H.J.; Won, D.H.; Kim, J.; Woo, S.I. Sulfur-doped g-C_3N_4/$BiVO_4$ composite photocatalyst for water oxidation under visible light. *Chem. Mater.* **2016**, *28*, 1318–1324. [CrossRef]
10. He, F.; Chen, G.; Miao, J.W.; Wang, Z.X.; Su, D.M.; Liu, S.; Cai, W.Z.; Zhang, L.P.; Hao, S.; Liu, B. Sulfur-Mediated self-templating synthesis of tapered C-PAN/g-C_3N_4 composite nanotubes toward efficient photocatalytic H_2 evolution. *ACS Energy Lett.* **2016**, *1*, 969–975. [CrossRef]
11. Zada, A.; Humayun, M.; Raziq, F.; Zhang, X.L.; Qu, Y.; Bai, L.L.; Qin, C.L.; Jing, L.Q.; Fu, H.G. Exceptional visible-light-driven cocatalyst-free photocatalytic activity of g-C_3N_4 by well designed nanocomposites with plasmonic Au and SnO_2. *Adv. Energy Mater.* **2016**, *6*. [CrossRef]
12. Giannakopoulou, T.; Papailias, I.; Todorova, N.; Boukos, N.; Liu, Y.; Yu, J.G.; Trapalis, C. Tailoring the energy band gap and edges' potentials of g-C_3N_4/TiO_2 composite photocatalysts for NOx removal. *Chem. Eng. J.* **2017**, *310*, 571–580. [CrossRef]
13. Sridharan, K.; Jang, E.; Park, T.J. Novel visible light active graphitic C_3N_4–TiO_2 composite photocatalyst: Synergistic synthesis, growth and photocatalytic treatment of hazardous pollutants. *Appl. Catal. B Environ.* **2013**, *142*, 718–728. [CrossRef]

14. She, X.J.; Xu, H.; Wang, H.F.; Xia, J.X.; Song, Y.H.; Yan, J.; Xu, Y.G.; Zhang, Q.; Du, D.L.; Li, H.M. Controllable synthesis of CeO_2/g-C_3N_4 composites and their applications in the environment. *Dalton Trans.* **2015**, *44*, 7021–7031. [CrossRef] [PubMed]
15. Tian, N.; Huang, H.W.; Liu, C.Y.; Dong, F.; Zhang, T.R.; Du, X.; Yu, S.X.; Zhang, Y.H. In situ co-pyrolysis fabrication of CeO_2/g-C_3N_4 n–n type heterojunction for synchronously promoting photo-induced oxidation and reduction properties. *J. Mater. Chem. A* **2015**, *3*, 17120–17129. [CrossRef]
16. Li, M.L.; Zhang, L.X.; Fan, X.Q.; Zhou, Y.J.; Wu, M.Y.; Shi, J.L. Highly selective CO_2 photoreduction to CO over g-C_3N_4/Bi_2WO_6 composites under visible light. *J. Mater. Chem. A* **2015**, *3*, 5189–5196. [CrossRef]
17. Tian, Y.L.; Chang, B.B.; Lu, J.L.; Fu, J.; Xi, F.N.; Dong, X.P. Hydrothermal synthesis of graphitic carbon nitride–Bi_2WO_6 heterojunctions with enhanced visible light photocatalytic activities. *ACS Appl. Mater. Interfaces* **2013**, *5*, 7079–7085. [CrossRef] [PubMed]
18. Wang, H.H.; Lu, J.; Wang, F.Q.; Wei, W.H.; Chang, Y.; Dong, S.J. Preparation, characterization and photocatalytic performance of g-C_3N_4/Bi_2WO_6 composites for methyl orange degradation. *Ceram. Int.* **2014**, *40*, 9077–9086. [CrossRef]
19. Xiong, M.; Chen, L.; Yuan, Q.; He, J.; Luo, S.L.; Au, C.T.; Yin, S.F. Controlled synthesis of graphitic carbon nitride/beta bismuth oxide composite and its high visible-light photocatalytic activity. *Carbon* **2015**, *86*, 217–224. [CrossRef]
20. Sierra, M.; Borges, E.; Esparza, P.; Méndez-Ramos, J.; Martín-Gil, J.; Martín-Ramos, P. Photocatalytic activities of coke carbon/g-C_3N_4 and Bi metal/Bi mixed oxides/g-C_3N_4 nanohybrids for the degradation of pollutants in waste water. *Sci. Technol. Adv. Mater.* **2016**, *17*, 659–668. [CrossRef] [PubMed]
21. Nogueira, A.E.; Lopes, O.F.; Neto, A.B.S.; Ribeiro, C. Enhanced Cr(VI) photoreduction in aqueous solution using Nb_2O_5/CuO heterostructures under UV and visible irradiation. *Chem. Eng. J.* **2017**, *312*, 220–227. [CrossRef]
22. Banerjee, A.; Singh, U.; Aravindan, V.; Srinivasan, M.; Ogale, S. Synthesis of CuO nanostructures from Cu-based metal organic framework (MOF-199) for application as anode for Li-ion batteries. *Nano Energy* **2013**, *2*, 1158–1163. [CrossRef]
23. Zhang, Q.B.; Zhang, K.L.; Xu, D.G.; Yang, G.C.; Huang, H.; Nie, F.D.; Liu, C.M.; Yang, S.H. CuO nanostructures: Synthesis, characterization, growth mechanisms, fundamental properties, and applications. *Prog. Mater Sci.* **2014**, *60*, 208–337. [CrossRef]
24. Zhang, S.Y.; Liu, H.; Liu, P.F.; Yang, Z.H.; Feng, X.; Huo, F.W.; Lu, X.H. A template-free method for stable CuO hollow microspheres fabricated from a metal organic framework (HKUST-1). *Nanoscale* **2015**, *7*, 9411–9415. [CrossRef] [PubMed]
25. Zhu, J.W.; Zeng, G.Y.; Nie, F.D.; Xu, X.M.; Chen, S.; Han, Q.F.; Wang, X. Decorating graphene oxide with CuO nanoparticles in a water-isopropanol system. *Nanoscale* **2010**, *2*, 988–994. [CrossRef] [PubMed]
26. Zabilskiy, M.; Djinović, P.; Erjavec, B.; Dražić, G.; Pintar, A. Small CuO clusters on CeO_2 nanospheres as active species for catalytic N_2O decomposition. *Appl. Catal. B Environ.* **2015**, *163*, 113–122. [CrossRef]
27. Wang, J.P.; Xu, H.; Qian, X.F.; Dong, Y.Y.; Gao, J.K.; Qian, G.D.; Yao, J.M. Direct synthesis of porous nanorod-type graphitic carbon nitride/CuO composite from Cu–melamine supramolecular framework towards enhanced photocatalytic performance. *Chem. Asian J.* **2015**, *10*, 1276–1280. [CrossRef] [PubMed]
28. Chandru, R.A.; Patra, S.; Oommen, C.; Munichandraiah, N.; Raghunandan, B.N. Exceptional activity of mesoporous β-MnO_2 in the catalytic thermal sensitization of ammonium perchlorate. *J. Mater. Chem.* **2012**, *22*, 6536–6538. [CrossRef]
29. Yuan, Y.; Jiang, W.; Wang, Y.J.; Shen, P.; Li, F.S.; Li, P.Y.; Zhao, F.Q.; Gao, H.X. Hydrothermal preparation of Fe_2O_3/graphene nanocomposite and its enhanced catalytic activity on the thermal decomposition of ammonium perchlorate. *Appl. Surf. Sci.* **2014**, *303*, 354–359. [CrossRef]
30. Tan, L.H.; Xu, J.H.; Zhang, X.J.; Hang, Z.S.; Jia, Y.Q.; Wang, S.B. Synthesis of g-C_3N_4/CeO_2 nanocomposites with improved catalytic activity on the thermal decomposition of ammonium perchlorate. *Appl. Surf. Sci.* **2015**, *356*, 447–453. [CrossRef]
31. Yu, J.G.; Ran, J.R. Facile preparation and enhanced photocatalytic H_2-production activity of $Cu(OH)_2$ cluster modified TiO_2. *Energy Environ. Sci.* **2011**, *4*, 1364–1371. [CrossRef]
32. Dong, M.; Wu, J.; Gao, M.C.; Xin, Y.J.; Ma, T.J.; Sun, Y.Y. Fabrication of Z-scheme g-C_3N_4/RGO/Bi_2WO_6 photocatalyst with enhanced visible-light photocatalytic activity. *Chem. Eng. J.* **2016**, *290*, 136–146.

33. Chetia, T.R.; Ansari, M.S.; Qureshi, M. Graphitic carbon nitride as a photovoltaic booster in quantum dot sensitized solar cells: A synergistic approach for enhanced charge separation and injection. *J. Mater. Chem. A* **2016**, *4*, 5528–5541. [CrossRef]
34. Auxilia, F.M.; Ishihara, S.; Mandal, S.; Tanabe, T.; Saravanan, G.; Ramesh, G.V.; Umezawa, N.; Hara, T.; Xu, Y.; Hishita, S. Catalysis: Low-temperature remediation of NO catalyzed by interleaved CuO nanoplates. *Adv. Mater.* **2014**, *26*, 4481–4485. [CrossRef] [PubMed]
35. Duan, X.C.; Huang, H.; Xiao, S.H.; Deng, J.W.; Zhou, G.; Li, Q.H.; Wang, T.H. 3D hierarchical CuO mesocrystals from ionic liquid precursors: Towards better electrochemical performance for Li-ion batteries. *J. Mater. Chem. A* **2016**, *4*, 8402–8411. [CrossRef]
36. Hong, Y.Z.; Li, C.C.; Zhang, G.Y.; Meng, Y.D.; Yin, B.X.; Zhao, Y.; Shi, W.D. Efficient and stable Nb_2O_5 modified g-C_3N_4 photocatalyst for removal of antibiotic pollutant. *Chem. Eng. J.* **2016**, *299*, 74–84. [CrossRef]
37. Fang, S.; Xia, Y.; Lv, K.L.; Li, Q.; Sun, J.; Li, M. Effect of carbon-dots modification on the structure and photocatalytic activity of g-C_3N_4. *Appl. Catal. B Environ.* **2016**, *185*, 225–232. [CrossRef]
38. Liu, Q.; Guo, Y.R.; Chen, Z.H.; Zhang, Z.G.; Fang, X.M. Constructing a novel ternary Fe(III)/graphene/g-C_3N_4 composite photocatalyst with enhanced visible-light driven photocatalytic activity via interfacial charge transfer effect. *Appl. Catal. B Environ.* **2016**, *183*, 231–241. [CrossRef]
39. Gao, H.L.; Yan, S.C.; Wang, J.J.; Zou, Z.G. Ion coordination significantly enhances the photocatalytic activity of graphitic-phase carbon nitride. *Dalton Trans.* **2014**, *43*, 8178–8183. [CrossRef] [PubMed]
40. Cao, S.W.; Low, J.X.; Yu, J.G.; Jaroniec, M. Polymeric photocatalysts based on graphitic carbon nitride. *Adv. Mater.* **2015**, *27*, 2150–2176. [CrossRef] [PubMed]
41. Fang, J.W.; Fan, H.Q.; Zhu, Z.Y.; Kong, L.B.; Ma, L.T. "Dyed" graphitic carbon nitride with greatly extended visible-light-responsive range for hydrogen evolution. *J. Catal.* **2016**, *339*, 93–101. [CrossRef]
42. Zhu, T.T.; Song, Y.H.; Ji, H.Y.; Xu, Y.G.; Song, Y.X.; Xia, J.X.; Yin, S.; Li, Y.P.; Xu, H.; Zhang, Q. Synthesis of g-C_3N_4/Ag_3VO_4 composites with enhanced photocatalytic activity under visible light irradiation. *Chem. Eng. J.* **2015**, *44*, 96–105. [CrossRef]
43. He, Y.M.; Wang, Y.; Zhang, L.H.; Teng, B.T.; Fan, M.H. High-efficiency conversion of CO_2 to fuel over ZnO/g-C_3N_4 photocatalyst. *Appl. Catal. B Environ.* **2015**, *168*, 1–8. [CrossRef]
44. Wu, W.T.; Zhang, J.Q.; Fan, W.Y.; Li, Z.T.; Wang, L.Z.; Li, X.M.; Wang, Y.; Wang, R.Q.; Zheng, J.T.; Wu, M.B. Remedying defects in carbon ntride to improve both photooxidation and H_2 generation efficiencies. *ACS Catal.* **2016**, *6*, 3365–3371. [CrossRef]
45. Huang, Z.A.; Sun, Q.; Lv, K.L.; Zhang, Z.H.; Mei, L.; Bing, L. Effect of contact interface between TiO_2 and g-C_3N_4 on the photoreactivity of g-C_3N_4/TiO_2 photocatalyst: (001) vs. (101) facets of TiO_2. *Appl. Catal. B Environ.* **2015**, *164*, 420–427. [CrossRef]
46. Zhang, Y.F.; Meng, C.G. Facile fabrication of Fe_3O_4 and Co_3O_4 microspheres and their influence on the thermal decomposition of ammonium perchlorate. *J. Alloys Compd.* **2016**, *674*, 259–265. [CrossRef]
47. Zhang, W.J.; Li, P.; Xu, H.B.; Sun, R.D.; Qing, P.H.; Zhang, Y. Thermal decomposition of ammonium perchlorate in the presence of $Al(OH)_3$·$Cr(OH)_3$ nanoparticles. *J. Hazard. Mater.* **2014**, *268*, 273–280. [CrossRef] [PubMed]
48. Fertassi, M.A.; Alali, K.T.; Liu, Q.; Li, R.Z.; Liu, P.G.; Liu, J.Y.; Liu, L.H.; Wang, J. Catalytic effect of CuO nanoplates, a graphene (G)/CuO nanocomposite and an Al/G/CuO composite on the thermal decomposition of ammonium perchlorate. *RSC Adv.* **2016**, *6*, 74155–74161. [CrossRef]
49. Shi, W.L.; Guo, F.; Chen, J.B.; Che, G.B.; Lin, X. Hydrothermal synthesis of $InVO_4$/Graphitic carbon nitride heterojunctions and excellent visible-light-driven photocatalytic performance for rhodamine B. *J. Alloys Compd.* **2014**, *612*, 143–148. [CrossRef]
50. Hu, B.; Cai, F.P.; Chen, T.J.; Fan, M.S.; Song, C.J.; Yan, X.; Shi, W.D. Hydrothermal synthesis g-C_3N_4/Nano-$InVO_4$ nanocomposites and enhanced photocatalytic activity for hydrogen production under visible light irradiation. *ACS Appl. Mater. Interfaces* **2015**, *7*, 18247–18256. [CrossRef] [PubMed]
51. Tang, G.; Tian, S.Q.; Zhou, Z.X.; Wen, Y.W.; Pang, A.M.; Zhang, Y.G.; Zeng, D.W.; Li, H.T.; Shan, B.; Xie, C.S. ZnO micro/nanocrystals with tunable exposed (0001) facets for enhanced catalytic activity on the thermal decomposition of ammonium perchlorate. *J. Phys. Chem. C* **2014**, *118*, 11833–11841. [CrossRef]
52. Boldyrev, V.V. Thermal decomposition of ammonium perchlorate. *Thermochim. Acta* **2006**, *443*, 1–36. [CrossRef]

53. Chen, L.J.; Li, L.P.; Li, G.S. Synthesis of CuO nanorods and their catalytic activity in the thermal decomposition of ammonium perchlorate. *J. Alloys Compd.* **2008**, *464*, 532–536. [CrossRef]
54. Su, F.Z.; Antonietti, M.; Wang, X.C. mpg-C_3N_4 as a solid base catalyst for Knoevenagel condensations and transesterification reactions. *Catal. Sci. Technol.* **2012**, *43*, 1005–1009. [CrossRef]
55. Li, Q.; He, Y.; Peng, R.F. Graphitic carbon nitride (g-C_3N_4) as a metal-free catalyst for thermal decomposition of ammonium perchlorate. *RSC Adv.* **2015**, *5*, 24507–24512. [CrossRef]
56. Li, Q.; He, Y.; Peng, R.F. One-step synthesis of SnO_2 nanoparticles-loaded graphitic carbon nitride and their application in thermal decomposition of ammonium perchlorate. *New J. Chem.* **2015**, *39*, 8703–8707. [CrossRef]